Microfluid Nanofluid (2013) 14:845–858
DOI 10.1007/s10404-012-1114-4

RESEARCH PAPER

Capillary self-alignment of polygonal chips: a generalization for the shift-restoring force

Jean Berthier · Sébastien Mermoz · Kenneth Brakke · Loic Sanchez · Christian Frétigny · Léa Di Cioccio

Received: 31 July 2012 / Accepted: 21 November 2012 / Published online: 12 December 2012

Abstract Capillary-driven self-alignment using droplets is currently extensively investigated for self-assembly and microassembly technology. In this technique, surface tension forces associated to capillary pinning create restoring forces and torques that tend to bring the moving part into the alignment. So far, most studies have addressed the problem of square chip alignment on a dedicated patch of a wafer, aiming to achieve 3D microelectronics. In this study, we investigate the shift-restoring forces for more complex moving parts such as regular—convex and non-convex—polygons and regular polygons with regular polygonal cavities. A closed-form approximate expression is derived for each of these polygonal geometries; this expression agrees with the numerical results obtained with the Surface Evolver software. For small shifts, it is found that the restoring force does not depend on the shift direction or on the polygonal shape. In order to tackle the problem of microsystem packaging, an extension of the theory is done for polygonal shapes pierced with connection vias (channels), and a closed form of the shift-restoring force is derived for these geometries and again checked against the numerical model. In this case, the restoring force depends on the shift direction. Finally, a non-dimensional number, the shift number, is proposed that indicates the isotropic or anisotropic behavior of the chip according to the shift direction.

Keywords Capillarity · Self-alignment · Polygonal chip · 3-D microelectronics · Shift-restoring force

J. Berthier (✉)
Department of Biotechnology, CEA-Leti,
17 Avenue des Martyrs, 38054 Grenoble, France
e-mail: jean.berthier@cea.fr

S. Mermoz
STMicroelectronics, 850 rue Jean Monnet,
38926 Crolles Cedex, France
e-mail: sebastien.mermoz@cea.fr

K. Brakke
Mathematics Department, Susquehana University,
514 University Avenue, Selingrove, PA 17870, USA
e-mail: brakke@susqu.edu

L. Sanchez · L. D. Cioccio
Department of Microelectronics, CEA-Leti,
17 Avenue des Martyrs, 38054 Grenoble, France
e-mail: loic.sanchez@cea.fr

L. D. Cioccio
e-mail: lea.dicioccio@cea.fr

C. Frétigny
UPMC/CNRS/ESPCI PPMD UMR 7615,
Physico-Chimie des Polymeres et des Milieux Disperses,
10 rue Vauquelin, 75231 Paris, Cedex 05, France
e-mail: christian.fretigny@espci.fr

1 Introduction

Capillary-driven self-alignment using droplets, or capillary self-assembly (CSA), is currently extensively investigated for self-assembly and microassembly technology (Martin et al. 2001; Whitesides and Boncheva 2002; Zheng and Jacobs 2005; Pelesko 2007; Böhringer 2008; Fukushima et al. 2009; Mastrangeli et al. 2009; Sariola et al. 2010; Berthier et al. 2010; Lambert et al. 2010; Chang et al. 2011; Sariola et al. 2011; Arutinov et al. 2012). In this technique, surface tension forces associated to capillary pinning create restoring forces and torques that tend to bring the moving part into alignment. In the field of 3D microelectronics, the method aims to be an alternate approach to the "pick and place" approach. In the capillary technique, the chip is

deposited on top of a water droplet and is brought into alignment by the action of capillary forces, due to the liquid interface tending to minimize its free area (Berthier and Brakke 2012). After alignment, which is fast, evaporation brings the chip into contact with the pad on the wafer, and direct bonding is possible if the two surfaces are sufficiently hydrophilic (Tong and Gösele 1999; Zheng and Jacobs 2005; Fukushima et al. 2009; Moriceau et al. 2010). A sketch of the process is shown in Fig. 1.

It is expected that self-alignment methods could be faster and more precise than the conventional robotic method. Developments have been fast, and it has been found that a square chip can be aligned by the action of restoring forces and torques if certain precautions are taken (Berthier et al. 2011; Mermoz et al. 2011). A review of the different concepts for 3D integration has recently been published by Lee et al. (2011).

Following the early investigations of the Whitesides group (Whitesides and Boncheva 2002; Boncheva et al. 2003), many different investigations have started: Knuesel and colleagues have used the method for the assembly of segmented monocrystalline solar cells (Knuesel and Jacobs 2010), Avital and Zussman have developed CSA methods for fluidic assembly of optical components (Avital and Zussman 2006), Zhang and colleagues have investigated the CSA of drosophila embryos on 2-D arrays of hydrophobic sites on a silicon substrate in water (Zhang et al. 2005), Stauth and Parviz have developed the self-assembly of single-crystal silicon circuits on plastic (Stauth and Parviz 2006), Takei and colleagues have obtained a microprism by capillary arrangement of two disks on a liquid droplet (Takei et al. 2011), and Fukushima and colleagues have studied the use of CSA for microsystem packaging (Fukushima et al. 2011). These investigations have been mainly experimental, except for the works of Lienemann et al. (2004), Zheng and Jacobs (2005) and Berthier et al. (2010, 2011). In the field of parallel liquid CSA, the shapes investigated are nearly uniquely squares and rectangles, except for some experimental investigations on hexagonal chips (Srinivasan et al. 2001), square cavity, and U-shaped microsystems (Fukushima et al. 2011). Note that self-assembly could be assisted by electro-capillary methods, such as that described by Wang et al. (2012). However, in order to facilitate future industrial processes, we have preferred to follow a purely passive approach.

In this study, we base our approach on the early work from Lienemann et al. (2004) and we extend it to develop a novel theoretical and numerical approach to the shift-restoring forces for polygonal chips. Our aim is to be able to estimate the shift- restoring force for different geometrical shapes of the moving part (and its identical fixed pad) composed of convex and concave polygons. It is shown that the analytical approach for the shift-restoring force using the deformation of flat facets agrees with the numerical results of the Surface Evolver software. Hence, we can derive the restoring forces for more realistic shapes such as polygons with cavities and for the double-U geometry investigated by Fukushima et al. (2011) shown in Fig. 2.

We make the assumption that the chip stays parallel to the substrate at all times during the alignment process: in the shift mode, it is just translated horizontally from its counterpart. Moreover, in this first analysis we assume that the liquid film perfectly wets both chip and pad, and stays pinned on all edges. It is clear that the wetting and pinning of the liquid film on reentrant angles has to be carefully investigated. It will be examined later in a further work, as was done for a square chip (Berthier et al. 2011).

In the particular case of regular polygons—convex or not—of the same perimeter, it is demonstrated that the magnitudes of the restoring forces at short range—small initial shift or at the end of the alignment process—are equal for all polygonal shapes. Also, the magnitude of the restoring force at small shift does not depend on the direction of the shift for these regular polygonal shapes. The theoretical results are in agreement with numerical results obtained with the Surface Evolver software (Brakke 1992). Moreover, it is shown that the approach can be extended to polygonal chips with polygonal cavities, such as those used by Fukushima et al. (2011) to seal microsystems. If connection vias or microchannels pierce the sides of the chip, the isotropic behavior is lost, and the former analytical expression has to be corrected by an anisotropic factor. Finally, it is shown that anisotropic chip geometries have restoring forces different than regular shapes and the isotropicity is characterized by a non-dimensional number which we call the shift number.

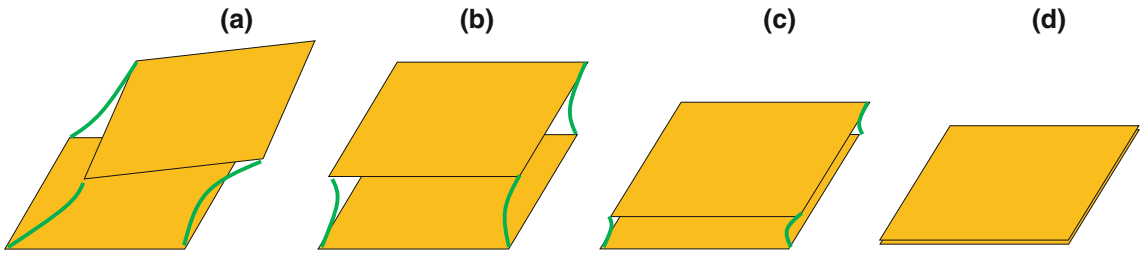

Fig. 1 Sketch of capillary self-alignment: **a** the moving part is deposited on the liquid; **b** capillary alignment; **c** evaporation; **d** contact and direct bonding

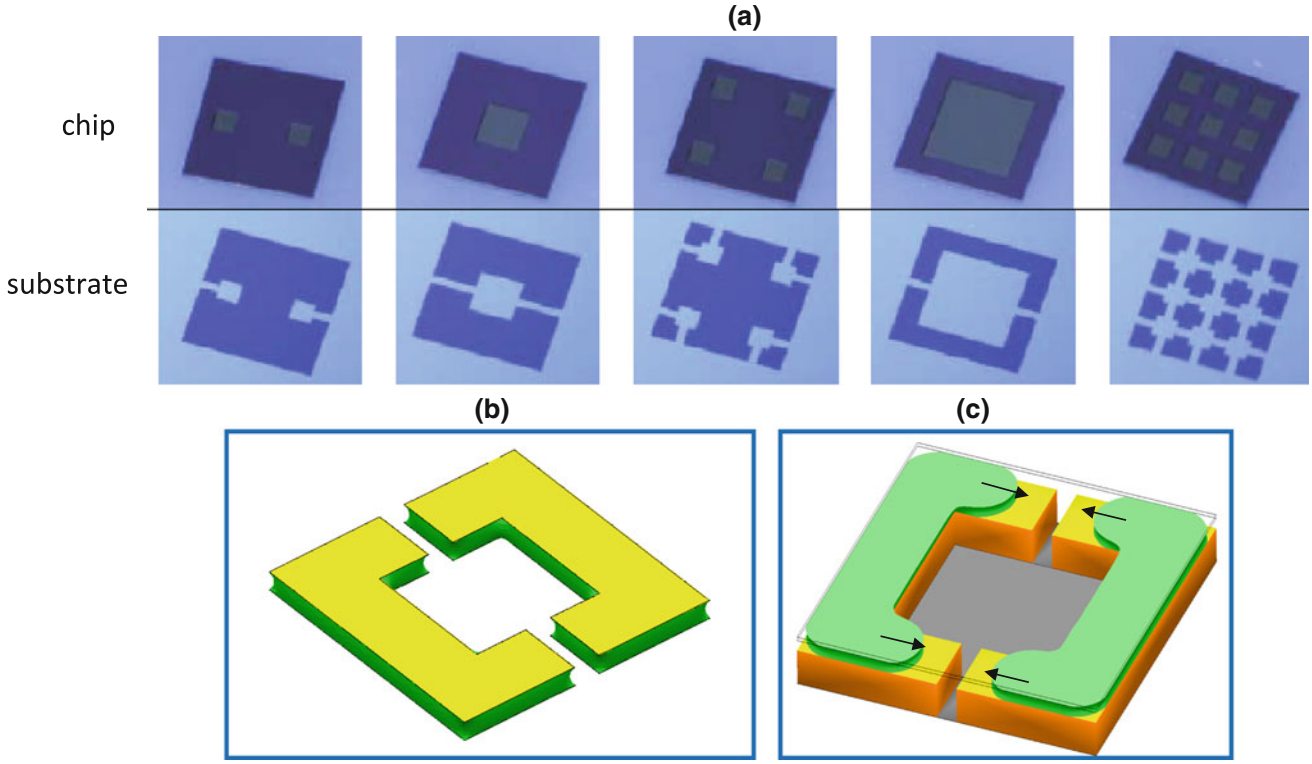

Fig. 2 **a**, **b** Cross-sectional SEM views of chips with cavities and channels (*Source* Fukushima et al. 2011; Reprinted with permission, © 2011, Micromachines); **c** liquid spreading on the chip top calculated with the numerical program Surface Evolver

2 Theory

Consider a chip in shape of a polygon and a shift x in the horizontal direction as sketched in Fig. 3. Edge number k has length s_k and angle from horizontal θ_k.

Now consider the deformation of one edge of length s and angle q, as shown in Fig. 4. The initial interface—assuming it is flat—has an area of

$$A_1 = sh \tag{1}$$

where h is the height of the liquid layer. The surface energy is then

$$E_1 = \gamma A_1 = \gamma s h \tag{2}$$

where γ is the surface tension. The shifted interface—still assuming it is flat—has an area of

$$A_2 = s\sqrt{h^2 + x^2 \sin^2 \theta} \tag{3}$$

where x is the shift. The corresponding surface energy is

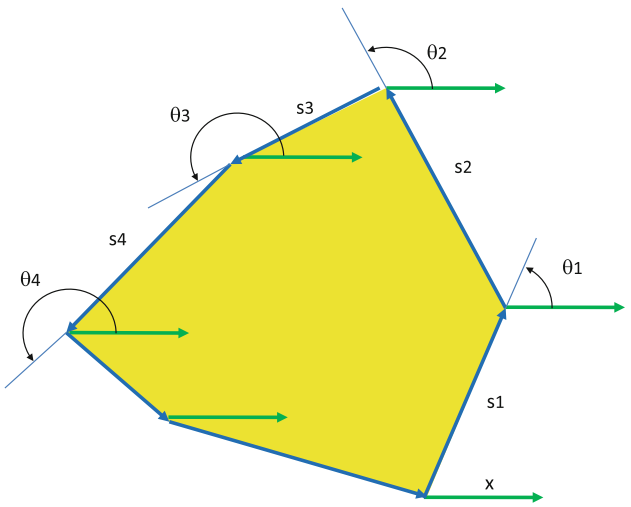

Fig. 3 Sketch of a polygon with shift direction

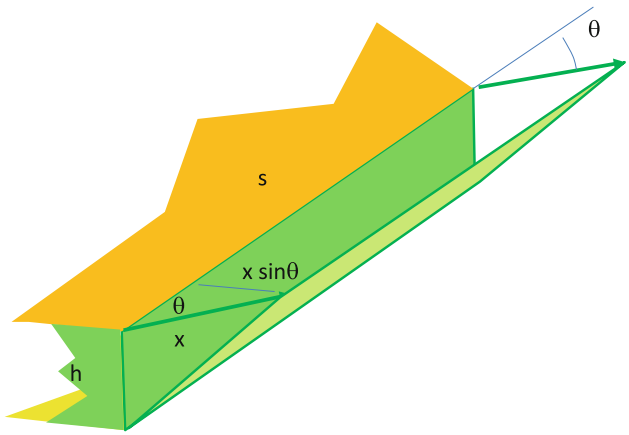

Fig. 4 Sketch of a shifted interface

$$E_2 = \gamma A_2 = \gamma s \sqrt{h^2 + x^2 \sin^2 \theta}. \quad (4)$$

Note that an interface parallel to the direction of the shift ($\theta = 0$) keeps the same surface area, and an interface perpendicular to the shift has the energy $E_2 = \gamma A_2 = \gamma s \sqrt{h^2 + x^2}$ which was found in our previous work in the case of a square chip and a shift perpendicular to an edge (Berthier et al. 2010). The restoring force corresponding to this single interface is

$$F = -\frac{\partial E_2}{\partial x} = -\gamma s x \sin^2 \theta \frac{1}{\sqrt{h^2 + x^2 \sin^2 \theta}}. \quad (5)$$

Approximating the surface energy of the whole interfacial area by the sum of the surface energy of all faces—i.e., not considering the inward curvature of the interface at the junction of two faces or any curvature in the middle of a face—the total surface energy after the shift is

$$E_2 = \sum_{i=1,n} E_i = \gamma A_2 = \gamma \sum_{i=1,n} s_i \sqrt{h^2 + x^2 \sin^2 \theta_i}. \quad (6)$$

The restoring force is then

$$F = \sum_{i=1,n} F_i = -\gamma x \sum_{i=1,n} s_i \sin^2 \theta_i \frac{1}{\sqrt{h^2 + x^2 \sin^2 \theta_i}}. \quad (7)$$

An interesting observation is that, when x is very small in comparison with h, relation (7) collapses to

$$F = -\gamma \frac{x}{h} \sum_{i=1,n} s_i \sin^2 \theta_i. \quad (8)$$

Relation (8) shows that when x is small, the restoring force is a linear function of x. On the other hand, if the shift x is large compared to the vertical dimension of the fluid layer h, then (7) collapses to

$$F = -\text{sign}(x) \gamma \sum_{i=1,n} s_i |\sin \theta_i|. \quad (9)$$

In this last case, the restoring force is constant. If we apply relation (8) and (9) to the case of the square, we retrieve the relations given in previous work (Berthier et al. 2010). A geometrical interpretation of (9) is given in "Appendix 1".

Consider now polygons, convex or not, with equal edges. Then, for all i we have $s_i = s$, and relation (8) becomes

$$F = -\gamma s \frac{x}{h} \sum_{i=1,n} \sin^2 \theta_i \quad (10)$$

Relation (10) can be simplified by introducing the polygon perimeter p and using the fact that the average of $\sin^2 \theta_i$ over equally spaced angles is $p/2s$ then:

$$F = -\gamma \frac{x}{h} \frac{p}{2} = -\gamma \frac{x}{\varepsilon} \quad (11)$$

where ε is the aspect ratio $2h/p$. An important remark is that the restoring force F at small range does not depend on the shift direction or on the shape of the polygon.

On the other hand, (9) becomes an asymptotic value for the shift-restoring force for large shifts:

$$F = -\text{sign}(x) \gamma s \sum_{i=1,n} |\sin \theta_i| \quad (12)$$

Note that the magnitude of the restoring force F in this latter expression depends on the polygonal shape and on the direction of the shift, but not on the magnitude of the shift. For a convex polygon, relation (12) is just the surface tension times twice the transverse width of the polygon, which is to be expected, since a large shift just stretches two horizontal surfaces, top and bottom, each of the width of the polygon.

3 Regular polygons (convex)

We investigate first the case of regular convex polygons. In "Appendix 2", it is shown that relation (12) for large shifts can be expressed by

$$F = -\frac{\gamma s}{2 \sin \frac{\pi}{n}} \sum_{i=1,n} \left| \left[\cos\left(2(i+1)\frac{\pi}{n}\right) - \cos\left(2i\frac{\pi}{n}\right) \right] \sin \alpha + \left[\sin\left(2(i+1)\frac{\pi}{n}\right) - \sin\left(2i\frac{\pi}{n}\right) \right] \cos \alpha \right| \quad (13)$$

where α is the shift angle. A non-dimensional expression for the force can be defined by

$$f = \frac{F}{\gamma p}. \quad (14)$$

And the asymptotic value of f—that we denote here the "shift number" Sf—is

$$Sf = \left|\frac{F}{\gamma p}\right| = \frac{1}{2n \sin \frac{\pi}{n}} \sum_{i=1,n} \left| \left[\cos\left(2(i+1)\frac{\pi}{n}\right) - \cos\left(2i\frac{\pi}{n}\right) \right] \sin \alpha + \left[\sin\left(2(i+1)\frac{\pi}{n}\right) \sin\left(2i\frac{\pi}{n}\right) \right] \cos \alpha \right| \quad (15)$$

The shift number Sf depends only on the number of edges n, i.e., the polygonal shape, and the shift direction α. It is a measure of the isotropic behavior of the chip. If Sf is invariant with α, the shift-restoring forces are isotropic. The shift numbers for 5 different regular polygons (equilateral triangle, square, pentagon, hexagon, and octagon) are shown in Fig. 5. The shift numbers are comprised between 0.5 and 0.7 in all cases. The square has the least isotropic behavior, with a maximum variation of the shift-restoring force of 30 % with the shift direction; the other

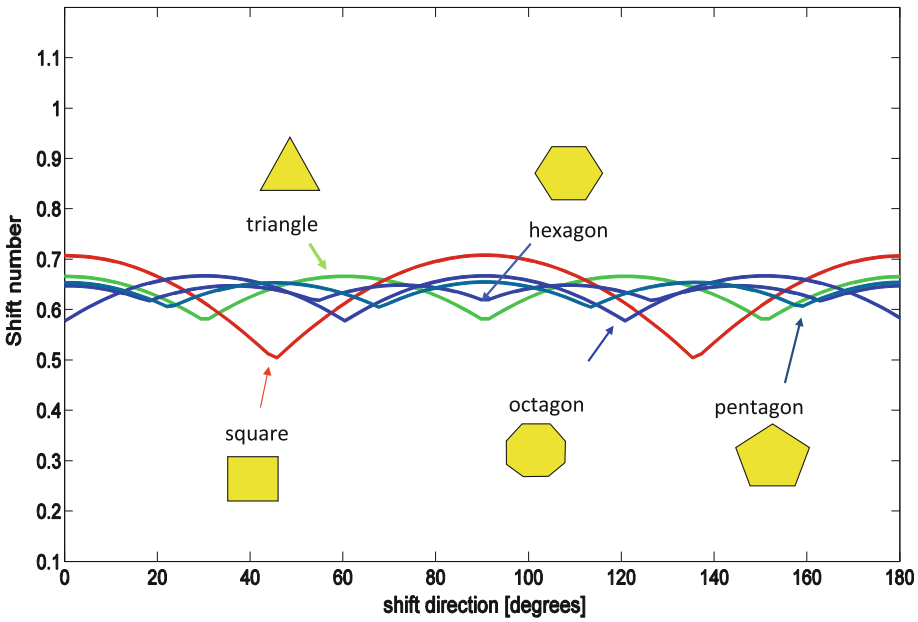

Fig. 5 Shift number as a function of the shift direction for five *regular polygons*

polygons show a variation of the shift-restoring force less than 15 %.

In conclusion, the theory predicts that the free energy and restoring forces are not very far apart for any shift angle or any regular polygonal shape. For small shifts it is predicted that they are equal, and similar for large shifts, because the shift number is similar for all shapes and all orientations.

4 Star polygons (regular and not convex)

Consider now the case of star polygons, a class of polygons defined in the reference Weisstein (2012) and let us examine the case of three polygons: pentagram, hexagram (star of David), and octagram. For small shifts ($x/h < 1/2$) relation (11) is valid. The case of large shift necessitates calculation of (12) for star polygons. For each type of polygon, two circles can be drawn, passing through the outer vertices and inner vertices. An external r_e and an internal radius r_i can then be defined as functions of the length of the edge s, and, using the same arguments developed in the "Appendix 2", the restoring force for large shifts can be expressed by

$$F = -\frac{\gamma}{2\sin\frac{\pi}{n}}\sum_{i=1,n}\left|\left[r_e\cos\left(2i\frac{\pi}{n}\right) - r_i\cos\left((2i-1)\frac{\pi}{n}\right)\right]\sin\alpha - \left[r_e\sin\left(2i\frac{\pi}{n}\right) - r_i\sin\left((2i-1)\frac{\pi}{n}\right)\right]\cos\alpha\right| \quad (16)$$

where the radii r_e and r_i are linear functions of s. The shift number showing the isotropic behavior of the chip is shown in Fig. 6. It varies between 0.55 and 0.65 according to the shift direction.

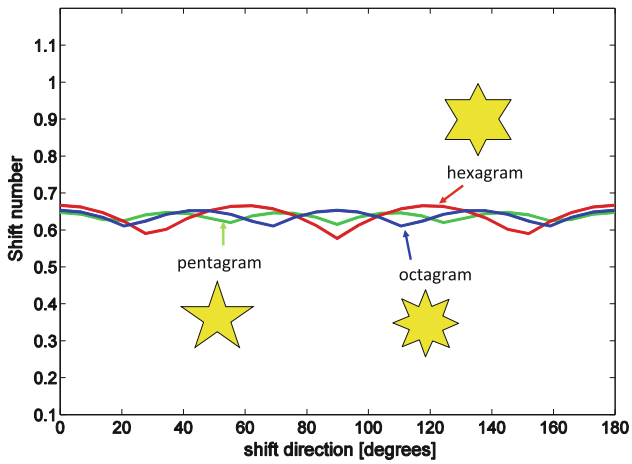

Fig. 6 Shift number for three different *star polygons*

5 Regular polygons with regular polygonal cavities

More complex surfaces have also been under scrutiny for capillary self-alignment. Sariola et al. (2011) have investigated the behavior of a capillary gripper with a cavity in its center, and Fukushima et al. (2011) are studying the alignment of microsystems cover for packaging. In a general approach, Böhringer et al. (2001) have shown that couples of composite substrates with hydrophilic and hydrophobic parts will reduce their energy when self-alignment is achieved, but even if alignment reduces the system energy, it cannot always be achieved when an energy saddle must be overcome.

In this section, we investigate the shift-restoring force for regular polygons—convex or not—with regular polygonal cavities. With the prerequisite of the same free perimeter p, relation (8) for small shift yields

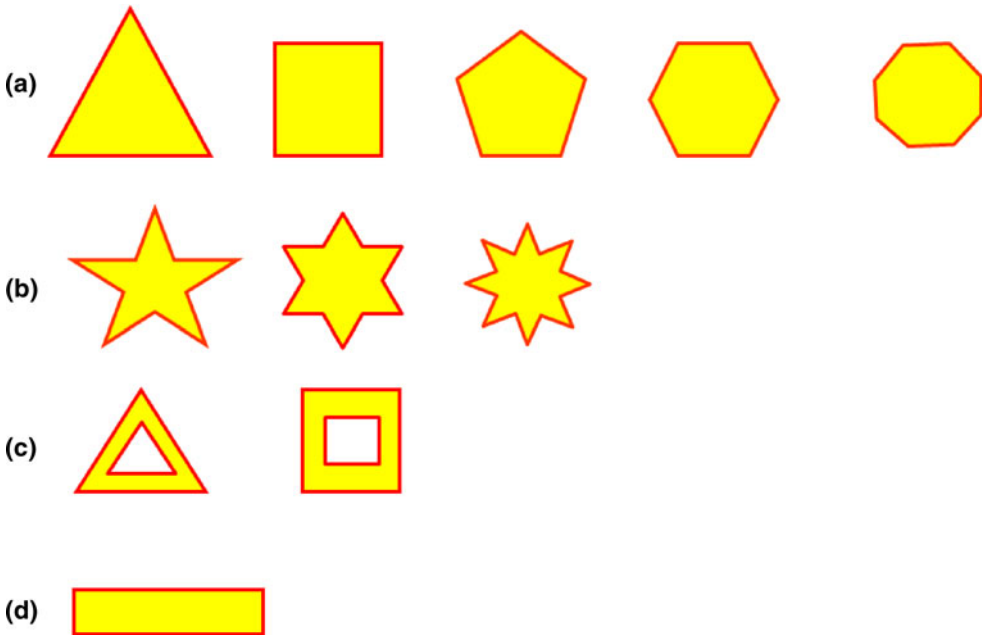

Fig. 7 The different polygons considered in the study: **a** *regular*, *convex polygons*; **b** *star polygons*, **c** *regular polygons* with regular polygonal cavity, and **d** *rectangle* of aspect ratio 2

$$F = -\gamma \frac{x}{h}\left(\sum_{i\subset \text{ext}} s_i \sin^2\theta_i + \sum_{i\subset \text{int}} s_i \sin^2\theta_i\right) \tag{17}$$

where ext refers to the external polygon and int to the internal polygon. This relation is similar to (11). Again, the restoring force at small shift does not depend on the shift direction or on the particular polygonal geometry. On the other hand, relation (9) for large shift yields

$$F = -\gamma\left(\sum_{i\subset \text{external}} s_i|\sin\theta_i| + \sum_{i\subset \text{internal}} s_i|\sin\theta_i|\right) \tag{18}$$

Consider the case of a regular polygon with side s and no cavity compared to one with a cavity homothetic to the external polygonal shape, with external side s_{ext} and internal side s_{int}. Assume that both geometries have the same total perimeter p. Then $s_{\text{ext}} + s_{\text{int}} = s = p/n$. Because the internal and external edges are aligned, the two terms of (18) with summation are equal. Finally, we obtain

$$F = -\gamma(s_{\text{ext}} + s_{\text{int}})\sum_i |\sin\theta_i| = -\gamma s \sum_i |\sin\theta_i| \tag{19}$$

The theory predicts that the full regular polygon and the polygon with homothetic cavity have the same restoring force, for the same total perimeter.

6 Numerical approach

The theoretical approach is an approximation since the interfaces have been considered flat. In order to take into account the real shape of the interfaces, we have used the numerical software Surface Evolver (Brakke 1992) to calculate the surface energy for different polygons (Fig. 7). First are regular polygons, i.e., convex polygons with $n = 1, 2, \ldots$ edges of same length. We limit ourselves to the equilateral triangle, square, pentagon, hexagon, and octagon. Second, we add the star polygons pentagram, hexagram, and octagram. Finally, we consider regular polygons with a regular polygonal cavity: a square with a square cavity, and a triangle with a triangular cavity. All these shapes can be considered "isotropic" as we will see in the following developments. In order to compare with an "anisotropic" shape, we also consider a rectangle of aspect ratio 2 or 1/2 (depending on its position in the coordinates system). Guided by (11), we use the same perimeter $p = 4$ cm in all cases.

The numerical protocol is the following: given an initial shift, the interface numerically adjusts to the real physical shape for that fixed shift. The corresponding surface energy is stored in a dedicated file. Then, the chip is freed to move incrementally. At each shift increment, the chip is fixed, the interface adjusts and the surface energy again is stored. The relation between the free energy and the shift is then plotted.

In this approach, we consider a uniform perimeter $p = 4 \times 10^{-2}$ m, this corresponds to a square of 1 cm × 1 cm. We set the liquid volume to $V = A\,h$, where A is the surface of the solid wetted by the liquid and h the vertical distance between the two solids. In our case $h \sim 400$ μm (there is a very small deviation due to the curvature of the interface). It is straightforward to show that the surface area of a regular polygon is given by the relation

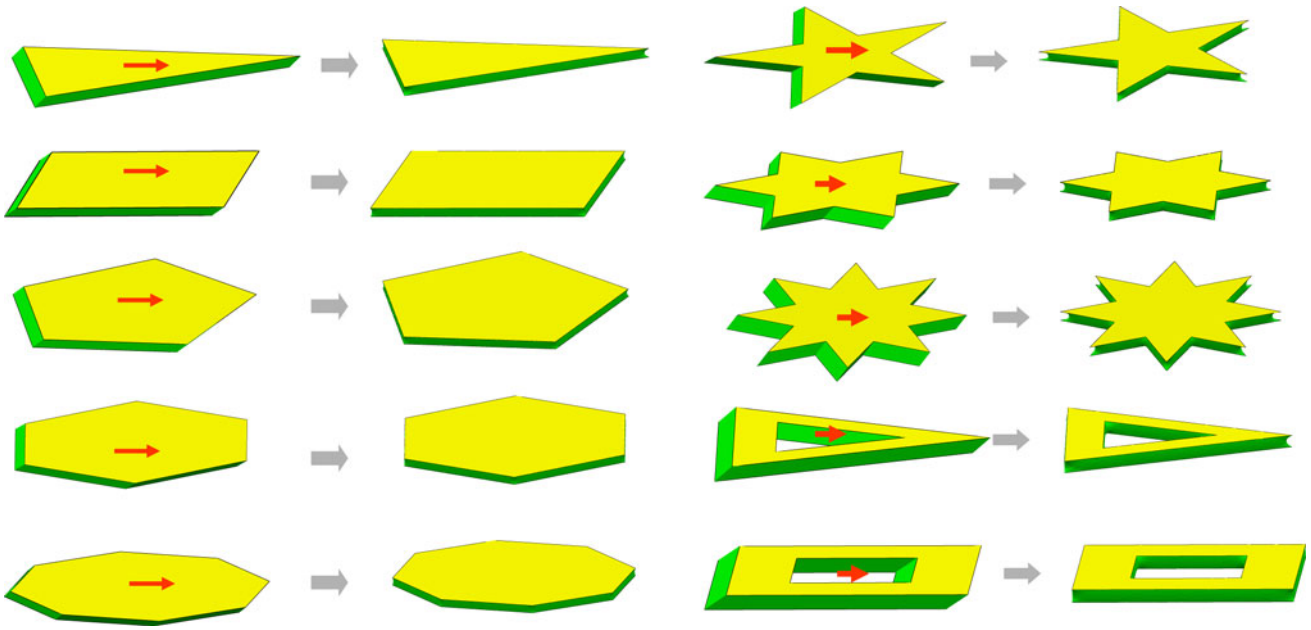

Fig. 8 Capillary self-alignment for *star polygons* and polygons with cavities, obtained with Surface Evolver

$$A = \frac{1}{4} n s^2 \cot\frac{\pi}{n} \tag{20}$$

where n the number of edges, and s the length of an edge.

Figure 8 shows different restoring processes for the different geometrical shapes considered.

7 Results

In this section, a comparison between the theoretical and numerical approaches is presented first. Then, the influence of the shift direction and chip shape on the free energy and on the restoring force is investigated. It is recalled that the restoring force is given by

$$F = -\frac{\partial E}{\partial x} \tag{21}$$

where E denotes the free energy and x the shift.

7.1 Comparison between theoretical and numerical results

A comparison between theoretical and numerical results for a 0° shift is shown in Fig. 9, for four different polygonal shapes (triangle, square, pentagon, and square with cavity). The agreement between theory and numerical model is good—which signifies that the hypothesis of flat surfaces is not too far from the reality—except maybe for the case of the square with a square cavity. In this case, the theory predicts the same restoring force as for the square. The discrepancy comes from the number of additional corners of the square with cavity. The real free surface becomes smaller for each additional corner, as is shown in Fig. 10.

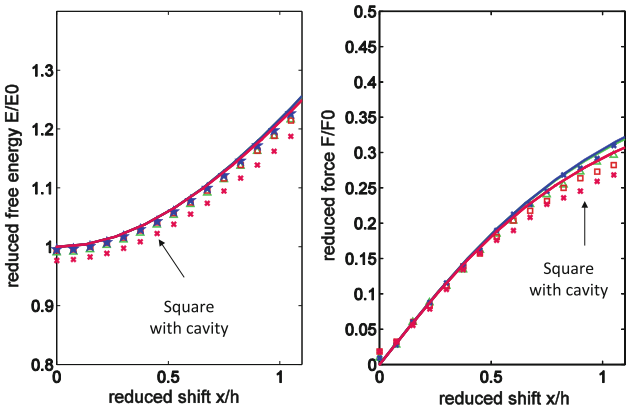

Fig. 9 Comparison between theory (*continuous lines*) and numerical model (*dotted lines*) for four different *polygonal shapes* with same perimeter: *equilateral triangle*, *square*, *pentagon*, and *square* with cavity. The references E_0 for energy and F_0 for the force are respectively $E_0 = \gamma\ h\ p$ and $F_0 = \gamma\ p$

The agreement also depends on the height h of the liquid layer. A large value of h would certainly increase the influence of the curvature of the interfaces. In the present case, the aspect ratio $\varepsilon = 2\ h/p$ of the thickness of the liquid layer and half the free perimeter is only 0.02. In the industrial process, a still smaller ratio is expected.

The preceding observation is still more acute in the case of star polygons: the presence of sharp angles and reentrant angles decreases the liquid interfacial area, and reduces the restoring force.

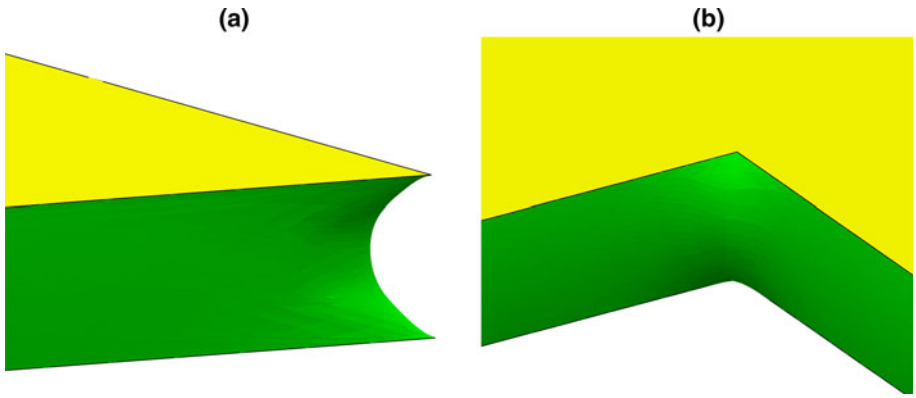

Fig. 10 View of the liquid interface in sharp or reentrant corners (Evolver)

Note that the shift between the energy curves in Figs. 9 and 11 has little influence on the restoring force for small shifts. It is due to the fact that the restoring force is the derivate of the energy and must be zero for $x/h = 0$.

In conclusion, the theory slightly overestimates the magnitude of the restoring force; but as the thickness of the liquid layer will be smaller in the real process, the difference between theory and numerical model is expected to be less than that shown in Fig. 11.

7.2 Influence of shift direction: isotropicity and anisotropicity

We analyze now the restoring force as a function of the shift direction. In Sect. 2 it has been found that for regular polygonal shapes, theory predict an independence of the shift-restoring force for small shifts ($x/h < 1/2$), and a moderate dependence for large shifts ($x/h > 1$). In this section, we use the Evolver to check these theoretical results.

Consider a square chip, and different directions of shift: $\alpha = 0$, 30, 45, 60, 90, 135, and 180°. A plot of the different restoring forces based on the general relation (7) is shown in Fig. 12. It is observed that when x/h is smaller than approximately 1/2, the restoring forces are all equal, as expected from the theory. The same results can be obtained for all the regular polygonal shapes. We deduce that when x/h is less than 1/2, the shift direction has no influence on the close range restoring forces for ''isotropic'' chips.

On the other hand, this is not the case with a ''non-isotropic'' polygonal shape, such as the rectangle. In Fig. 13, the shift number has been plotted as a function of the shift direction. Isotropic behavior is characterized by a shift number Sf of 0.62 corresponding to the octagon (regular polygon with many edges). An approximate isotropic situation occurs for shift numbers comprised between 0.55 and 0.7. The square can be considered as the limit. The shift number for a rectangle of aspect ratio 2

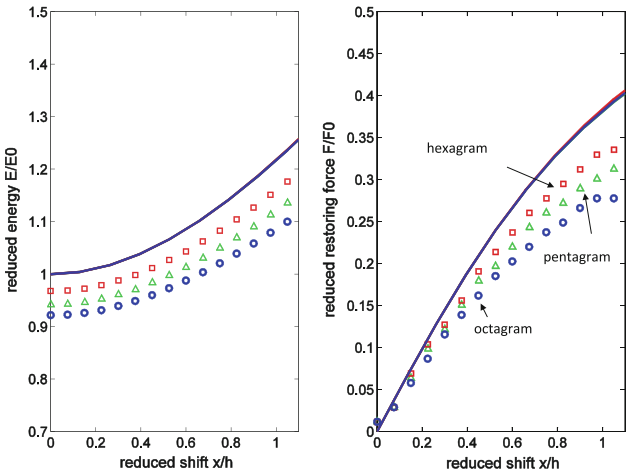

Fig. 11 Comparison between theory and numerical approach for star polygons (of same perimeter). *Continuous lines* correspond to the theory and *dotted lines* to Evolver calculations

varies between 0.3 and 0.75, which indicates an anisotropic behavior.

Note that, from "Appendix 1", the anisotropy is characterized by the ratio between the maximum and minimum cross lengths of the polygonal chip. In the case of a square, $L_{\max}/L_{\min} = \sqrt{2}$. More generally, it can be shown for regular polygons, that $L_{\max}/L_{\min} = 1/\cos(\pi/n)$.

7.3 Influence of polygonal shape

Let us now consider the different polygonal shapes of Fig. 7. Free surface energies are plotted in Fig. 14 as a function of a shift in the direction of the x-axis. From the figure, we deduce that all "isotropic" shapes—regular polygons, with a regular polygonal cavity, and star polygons—have a similar free surface energy, while the surface energy of the "anisotropic" rectangle notably differs from the other "isotropic" shapes.

Using (7), the same conclusion can be drawn for the shift-restoring force, as shown in Fig. 15.

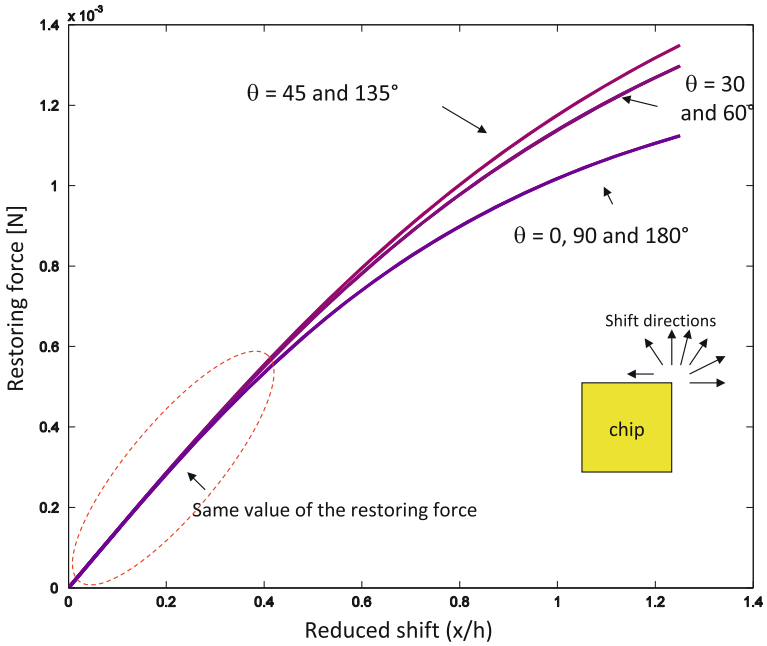

Fig. 12 Restoring forces as a function of the shift magnitude and direction (from Evolver)

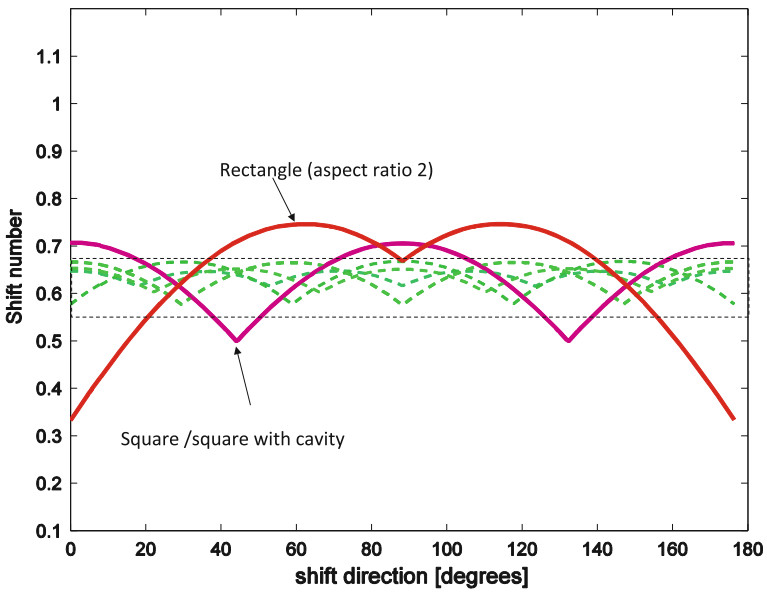

Fig. 13 Shift number as a function of the shift direction. The *green curves* correspond to the *equilateral triangle*, *pentagon*, *hexagon*, and *octagon*. Their behavior is nearly isotropic. The magenta curve corresponds to the *square shape*, at the limit of isotropic behavior, and the rectangle (*red line*) is fully anisotropic

7.4 Restoring force for small shifts

A perfect alignment is obtained when the force at small shift is sufficiently large; this can be characterized by determining the value of the derivative of the restoring force $\Delta = \mathrm{d}F/\mathrm{d}x|_{x=0}$ at the origin. The value of Δ has been obtained numerically from the Evolver values of Fig. 15. In Fig. 16, we have plotted the value of Δ for different polygonal geometries (with same free perimeter p) for very small shifts. For all regular polygonal geometries, the value of Δ converges toward the theoretical value $\Delta = \gamma\ p/2\ h = \gamma/\varepsilon$. On the other hand, the value of Δ for anisotropic geometries (here a rectangle) differs considerably from the theoretical results. This observation can be checked by referring to "Appendix 1": the restoring forces for x and y-direction shifts should be respectively proportional to the larger and smaller rectangle lengths.

Note that, from Fig. 15, the restoring force of regular polygons is larger than that of star polygons. This is due to the fact that, for a same perimeter, convex polygons have a larger circumcircle than concave polygons. Since the maximum restoring force is proportional to the maximum cross-length ($L_{\max}$), which is in turn twice the radius of the circumcircle for regular polygons, the restoring force is larger for convex shapes.

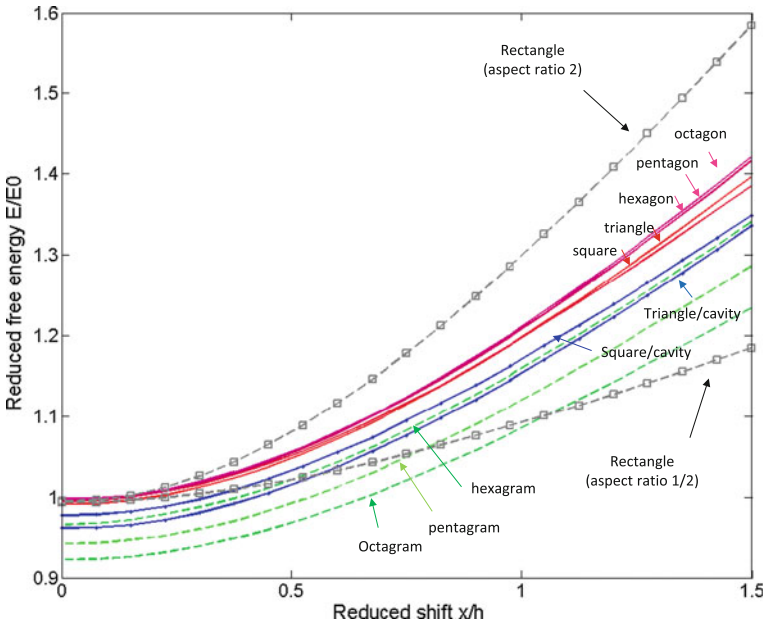

Fig. 14 Free energy versus shift for the different *polygonal shapes* obtained with the Surface Evolver

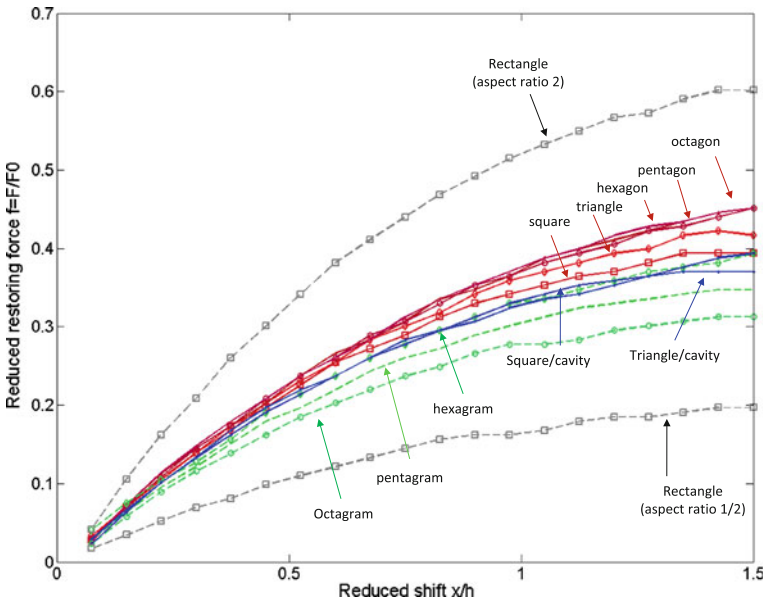

Fig. 15 Restoring force versus shift for different polygonal shapes with same free perimeter: The restoring forces are similar except for the anisotropic *rectangle*. Values obtained with the Evolver

8 Applications to microsystem packaging

In the preceding sections, we have shown the agreement between the analytical model based on flat interfaces and the numerical results from Evolver. Hence, we should be able to predict the shift-restoring force for more complicated shapes corresponding to more realistic cases.

In this section, we investigate the shift-restoring force in the geometry of a square microsystem where vias (channels) are opened on two opposite sides, similar to that proposed by Fukushima et al. (2011). As a matter of fact, for simplicity of handling the liquid spreading with Evolver, we have considered the same shapes for the chip and pad, whereas Fukushima considered side channels only in the fixed pad. Closed square shapes (with square cavities) have been investigated above, and we focus here on the anisotropy induced by the vias (Fig. 17). In this particular case, the width of the channels piercing the square is set to 1/10 of the external edge, and the cavity dimension is half that of the external dimension. In contrast with the preceding sections, we consider the same external dimensions of the square polygons in both cases, regardless of the difference between the free perimeters.

Figure 18 shows the restoring force as a function of the shift for the square chip (with square cavity) and for the

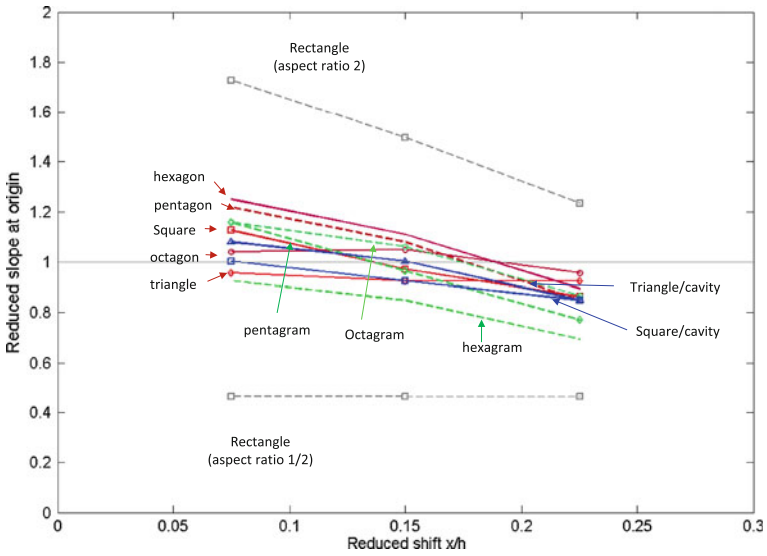

Fig. 16 Value of dF/dx at small shifts: all the regular polygons converge to the analytical value, while the anisotropic *rectangular shape* differs notably from this value (from Evolver)

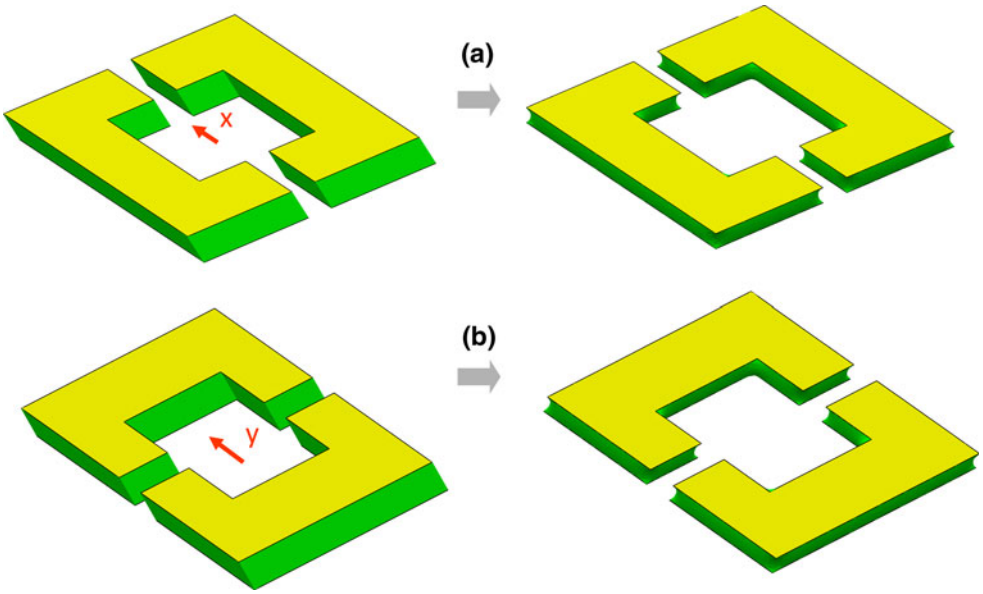

Fig. 17 Alignment of a *square* microsystem cover after a x-shift (**a**), and a y-shift (**b**)

cavity-chip along two perpendicular directions of the shift: first, the direction of the channels—x-direction—and second the direction perpendicular to the channels—y-direction. The anisotropy induced by the channels clearly appears in the figure.

In the same figure, we have also plotted two "modified" curves: the first one corresponds to the value of the force in the x-direction decreased by the missing interfacial area corresponding to the channel openings. If s_{ext} denotes the external square edge, s_{int} the internal square edge and w the width of the channels, we have

$$\frac{F_{\text{microsystem}}}{F_{\text{square}}} = \frac{2(s_{\text{ext}} + s_{\text{int}}) - 4w}{2(s_{\text{ext}} + s_{\text{int}})} = 1 - 2\frac{w}{(s_{\text{ext}} + s_{\text{int}})} \quad (22)$$

Conversely, in the case of a y-shift, the value of the restoring force is increased by

$$\frac{F_{\text{microsystem}}}{F_{\text{square}}} = \frac{2s_{\text{ext}} + 2s_{\text{int}} + 2(s_{\text{ext}} - s_{\text{int}})}{2s_{\text{ext}} + 2s_{\text{int}}} = \frac{2s_{\text{ext}}}{s_{\text{ext}} + s_{\text{int}}} \quad (23)$$

Using the values $w = s_{\text{ext}}/10$ and $s_{\text{ext}} = 2\ s_{\text{int}}$, we find the correction coefficients 13/15 and 4/3, which reproduce well the restoring force for a full (no channels) square with cavity. Hence, the restoring force at small shift can be approximated by

$$f = \frac{F}{\gamma p} = -\frac{x}{2h}\left(1 - 2\frac{w}{s_{\text{ext}} + s_{\text{int}}}\right) \quad (24)$$

for a shift along the channel axis, and

$$f = \frac{F}{\gamma p} = -\frac{x}{2h}\left(\frac{2s_{\text{ext}}}{s_{\text{ext}} + s_{\text{int}}}\right) \quad (25)$$

for a shift perpendicular to the channel axis. Relations (24)

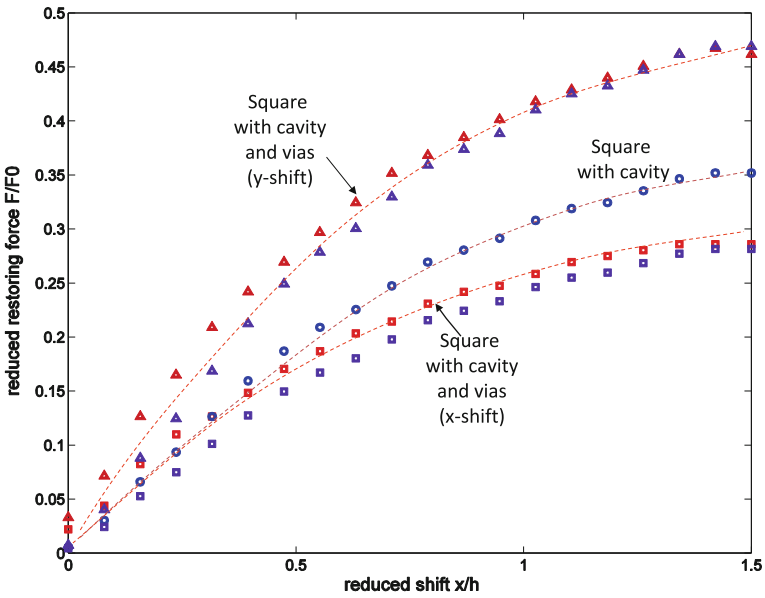

Fig. 18 Shift-restoring force: comparison between a square (with cavity) and a square (with cavity) pierced by two channels. The two channels induce anisotropy of the restoring forces. Calculation performed with Surface Evolver. The two additional *curves* are obtained from the *square* (with cavity) *curve* multiply by the corrective factors given by (22) and (23)

and (25) constitute the two limits for the restoring force at small shift for the pierced geometry considered here. The shift number is comprised between the values

$$\frac{x}{2h}\left(1-2\frac{w}{s_{\text{ext}}+s_{\text{int}}}\right)Sf_{\text{square}}<Sf<\frac{x}{2h}\left(\frac{2s_{\text{ext}}}{s_{\text{ext}}+s_{\text{int}}}\right)Sf_{\text{square}} \tag{26}$$

9 Conclusions and perspectives

In this study, an approximate closed form of the shift-restoring force has been derived from the assumption of flat interfaces for many different regular polygonal shapes. It has been shown that this analytical expression agrees well with the more detailed value produced by a numerical approach with the numerical software Surface Evolver. An interesting observation is that, for small shifts, the restoring force does not depend on the shift direction or on the polygonal shape. The restoring force is simply proportional to the surface tension, to the free perimeter and to the magnitude of the shift.

A non-dimensional number, the shift number, has been defined that characterizes the non-dimensional shift-restoring force, and the isotropicity of the system (for large shifts), i.e., the independence of the restoring force to the shift direction.

An extended expression of the shift-restoring force at close range has been derived for chips with cavity pierced by connection vias (microchannels), similar to that used for packaging microsystems. This extended relation has again been verified by a numerical approach.

So far, only the effect of the shift has been investigated. Twist, tilt, and roll restoring torques are still to be investigated, in order to have a complete assessment of the capillary effect on different polygonal chips.

Appendix 1: restoring forces for large shifts for any polygon

The force at large shift given by Eq. (9)

$$F=-\text{sign}(x)\gamma\sum_{i=1,n}s_i|\sin\theta_i| \tag{27}$$

has a geometrical significance. In Fig. 19 the projections of the edges s_i on the direction perpendicular to the shift show that

$$\sum_{i=1,n}s_i|\sin\theta_i|=2L_\perp \tag{28}$$

The restoring force at large shift is then

$$F=-\text{sign}(x)\gamma 2L_\perp \tag{29}$$

The magnitude of the restoring force is then comprised between the minimum and maximum cross lengths $L_{\min}$ and $L_{\max}$ times the surface tension γ (Fig. 19).

Appendix 2: restoring forces for large shifts for regular polygons

For a regular polygon with n edges of length s and free perimeter p, the following relation holds:

$$p=n\,s. \tag{30}$$

Using trigonometrical calculation, we find the value of the circumscribed circle to be

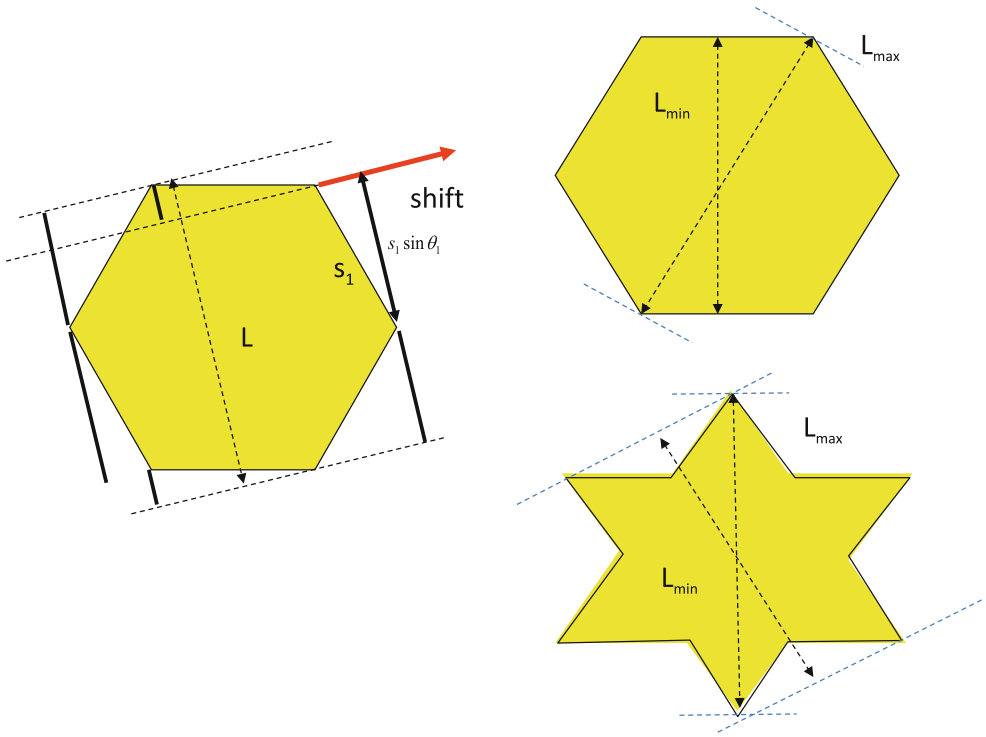

Fig. 19 *Left* projections on the direction perpendicular to the shift; *right* the two extrema for a hexagon and a hexagram

$$r = \frac{s}{2\sin\frac{\pi}{n}}. \tag{31}$$

Incidentally, the surface area of the solid wetted by the liquid can be expressed as a function of the perimeter p and the number of edges n:

$$A = \frac{1}{4}ns^2\cot\frac{\pi}{n} = \frac{1}{4}p^2\frac{1}{n}\cot\frac{\pi}{n}. \tag{32}$$

The coordinates of the polygon vertices are

$$S_i = r\left[\cos\left(2i\frac{\pi}{n}\right), \sin\left(2i\frac{\pi}{n}\right)\right] \tag{33}$$

where i is the vertex index. The oriented vector edges are then

$$\vec{s}_i = r\left[\cos\left(2(i+1)\frac{\pi}{n}\right) - \cos\left(2i\frac{\pi}{n}\right), \sin\left(2(i+1)\frac{\pi}{n}\right) - \sin\left(2i\frac{\pi}{n}\right)\right] \tag{34}$$

Let us assume that the shift direction is the unit vector defined by its polar angle α,

$$\vec{k} = [\cos\,\alpha, \sin\,\alpha]. \tag{35}$$

The cross-product between $\vec{s}_i$ and $\vec{k}$ produces the value of sin θ_i

$$\sin\,\theta_i = \frac{\vec{s}_i}{|\vec{s}_i|} \times \vec{k} = \frac{\vec{s}_i}{s_i} \times \vec{k}. \tag{36}$$

We finally find the expression

$$\sin\,\theta_i = \frac{1}{2\sin\frac{\pi}{n}}\left\{\left[\cos\left(2(i+1)\frac{\pi}{n}\right) - \cos\left(2i\frac{\pi}{n}\right)\right]\sin\,\alpha + \left[\sin\left(2(i+1)\frac{\pi}{n}\right) - \sin\left(2i\frac{\pi}{n}\right)\right]\cos\,\alpha\right\} \tag{37}$$

References

Arutinov G, Smit ECP, Mastrangeli M, van Heck G, van den Brand J, School HFM, Dietzel A (2012) Capillary self-alignment of mesoscopic foil components for sensor-systems-in-foil. J Micromec Microeng 22:115022. doi:10.1088/0960-1317/22/11/115022

Avital A, Zussman E (2006) Fluidic assembly of optical components. IEEE Trans Adv Packag 29(4):719–724. doi:10.1109/TADVP.2006.884810

Berthier J, Brakke K (2012) The physics of microdrops. Scrivener-Wiley publishing. doi:10.1002/9781118401323

Berthier J, Brakke K, Grossi F, Sanchez L, Di Cioccio L (2010) Self-alignment of silicon chips on wafers: a capillary approach. JAP 108:054905. doi:10.1063/1.3466782

Berthier J, Brakke K, Mermoz S, Sanchez L, Frétigny C, Di Cioccio L (2011) Self-alignment of silicon chips on wafers: a numerical investigation of the effect of spreading and wetting. Sens Transducers J 13:44–52

Böhringer KF (2008) Engineered self-assembly from nano to milli scales, in Multi-material micro manufacture. In: Dimov S, Menz W (eds) Whittles Publishing Ltd. doi:10.3850/978-981-6555

Böhringer KF, Srinivasan U, Howe RT (2001) Modeling of capillary forces and binding sites for fluidic self-assembly. Int Conf Micro Electro Mech Syst. doi:10.1.1.32.8332

Boncheva M, Bruzewicz DA, Whitesides GM (2003) Millimeter-scale self-assembly and its applications. Pure Appl Chem 75(5):621–630. doi:10.1109/MEMSYS.2012.5442454

Brakke K (1992) The surface evolver. Exp Math 1(2):141–165

Chang B, Sariola V, Aura S, Ras RHA, Klonner M, Lipsanen H, Zhou Q (2011) Capillary-driven self-assembly of microchips on oleophilic/oleophobic patterned surface using adhesive droplet in ambient air. APL 99:034104. doi:10.1063/1.3615053

Fukushima T, Tanaka T, Koyanagi M (2009) 3D system integration technology and 3D systems. In: Advanced metallization conference proceedings, pp 479–485

Fukushima T, Konno T, Iwata E, Kobayashi R, Kojima T, Murugesan M, Bea J-C, Lee K-W, Tanaka T, Koyanagi M (2011) Self-assembly of chip-size components with cavity structures: high-precision alignment and direct bonding without thermal compression for hetero integration. Micromachine 2:49–68. doi:10.3390/mi2010049

Knuesel RJ, Jacobs HO (2010) Self-assembly of microscopic chiplets at a liquid–liquid-solid interface forming a flexible segmented monocrystalline solar cell. PNAS 107(3):993. doi:10.1073/pnas.0909482107

Lambert P, Mastrangeli M, Valsamis J-B, Degrez G (2010) Spectral analysis and experimental study of lateral capillary dynamics for flip-chip applications. Microfluid Nanofluid 9:797–807. doi:10.1007/s10404-010-0595-2

Lee SH, Chen K-N, Lu JJ-Q (2011) Wafer-to-wafer alignment for three-dimensional integration: a review. J Microelec Syst 20(4):885. doi:10.1109/MEMS.2011.2148161

Lienemann J, Greiner A, Korvink JG (2004) Modeling, simulation, and experimentation of a promising new packaging technology: parallel fluidic self-assembly of microdevices. In: Baltes H, Fedder GK, Korvink JG (eds) Sensors update, vol 13. Wiley-VCH Verlag

Martin BR, Furnange DC, Jackson TN, Mallouk TE, Mayer TS (2001) Self-alignment of patterned wafers using capillary forces at a water-air interface. Adv Funct Mater 11(5):381–386. doi:10.1002/1616-3028(200110)11:5

Mastrangeli M, Abbasi S, Varel C, Van Hoof C, Celis J-P, Böhringer KF (2009) Self-assembly from milli- to nanoscales: methods and applications. J Micromech Microeng 19:083001. doi:10.1088/0960-1317/19/8/083001

Mermoz S, Sanchez L, Di Cioccio L, Berthier J, Deloffre E, Fretigny C (2011) Impact of containment and deposition method on sub-micron chip-to-wafer self-assembly yield. In: Proceedings of the 3DIC conference, Osaka, Japon, January 31–February 2

Moriceau H, Rieutord F, Fournel F, Le Tiec Y, Di Cioccio L, Morales C, Charvet AM, Deguet D (2010) Overview of recent direct wafer bonding advances and applications. Adv Nat Sci Nanosci Nanotechnol 1:043004. doi:10.1088/2043-6262/1/4/043004

Pelesko JA (2007) Self-assembly: the science of things that put themselves together. Chapman and Hall/CRC, London

Sariola V, Jääskeläinen M, Zhou Q (2010) Hybrid microassembly combining robotics and water droplet self-alignment. IEEE Trans Rob 26(6):965

Sariola V, Liimatainen V, Tolonen T, Udd R, Zhou Q (2011) Silicon capillary gripper with self-alignment capability. In: 2011 IEEE international conference on robotics and automation, Shanghai International Conference center, May 9–13, 2011, Shanghai, China

Srinivasan U, Liepmann D, Howe RT (2001) Microstructure to substrate self-assembly using capillary forces. J Microelectromech Syst 10:17–24. doi:10.1109/84.911087

Stauth SA, Parviz BA (2006) Self-assembled single-crystal silicon circuits on plastic. PNAS 103(38):13922. doi:10.1073/pnas.0602893103

Takei A, Yoshihata Y, Shimoyama I (2011) Microprism using capillary alignment. J Micromech Microeng 21:085009. doi:10.1088/0960-1317/21/8/085009

Tong QY, Gösele U (1999) Semiconductor wafer bonding. Wiley, Hoboken. doi:10.1146/annurev.matsci.28.1.215

Wang ZQ, Wang FC, Zhao YP (2012) Tap dance of water droplet. Proc R Soc A 468:2485–2495. doi:10.1098/rspa.2011.0679

Weisstein EW (2012) Star Polygon. MathWorld—A Wolfram Web Resource. http://mathworld.wolfram.com/StarPolygon.html

Whitesides GM, Boncheva M (2002) Beyond molecules: self-assembly of mesoscopic and macroscopic components. PNAS 99:4769–4774. doi:10.1073/pnas.082065899

Zhang XJ, Chen CC, Bernstein RW, Zappe S, Scott MP, Solgaard O (2005) Microoptical characterization and modeling of positioning forces on drosophila embryos self-assembled in two-dimensional arrays. J Microelectromech Syst 14(5):1187. doi:10.1109/JMEMS.2005.851834

Zheng W, Jacobs HO (2005) Fabrication of multicomponent microsystems by directed three-dimensional self-assembly. Adv Funct Mater 15:732. doi:10.1002/adfl.200400595